

Sep 2013

GLM

General Lake Model (GLM) –

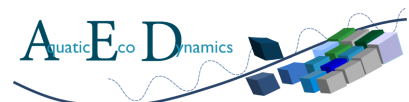
Model Overview and User Information

DRAFT v1.3.0

M.R. Hipsey, L.C. Bruce & D.P. Hamilton



THE UNIVERSITY OF
WESTERN AUSTRALIA
Achieve International Excellence



Summary

This document summarises the basis and operational details for the 1D lake water balance and vertical stratification model: GLM (The General Lake Model). GLM designed to be an open community model suited to environmental modelling studies where simulation of lakes or reservoirs is required. The model couples with the Framework for Aquatic Biogeochemical Models (FABM) for integrated simulations of lake and reservoir water quality and ecosystem health.

This manual summarises the surface exchange and ice-cover dynamics, vertical mixing and inflow/outflow models, including the numerical representation of the processes and the nature of the solution. A summary of typical parameter values for lakes and reservoirs collated from a range of sources is included. The final section provides an overview of setting up and running the model.

Contents

SUMMARY	2
CONTENTS	3
THE GENERAL LAKE MODEL (GLM)	4
OVERVIEW	4
MODEL DESCRIPTION	4
Layer structure	4
Energy Budget	4
Surface Mass Fluxes	5
Snow/Ice Model	6
Vertical mixing	8
Inflows and outflows	9
MODEL INPUT DATA REQUIREMENTS	10
GLM-FABM-AED SETUP	12
OVERVIEW	12
INPUT FILES	12
Physical model configuration: glm.nml	12
Meteorology: met.csv	13
Inflows: inflows.csv	14
Outflows: outflows.csv	14
RUNNING THE MODEL	15
OUTPUTS AND POST-PROCESSING	15
Live output plotting: plots.nml	15
Plotting in EXCEL	15
Plotting in MATLAB	15
Plotting with PyNCview	16
PARAMETER OPTIMISATION	16
EXAMPLES & SUPPORT	17
DOWNLOADS & ONLINE FORUM	17
FURTHER SUPPORT & DEVELOPMENT REQUESTS	17
EXAMPLES	17
Lake Kinneret	17
Lake Constance	17
REFERENCES	18

The General Lake Model (GLM)

Overview

The *General Lake Model* (GLM) is a one-dimensional vertical stratification hydrodynamic model driver for lakes. GLM computes vertical profiles of temperature, salinity and density by accounting for the effect of inflows/outflows, mixing and surface heating and cooling, including the effect of ice cover on heating and mixing of the lake.

Since the model is one-dimensional it assumes no horizontal variability so users must ensure the lake conditions match this one-dimensional assumption. The model is ideally suited to long-term investigations ranging from seasons to decades, and for coupling with biogeochemical models to explore the role that stratification and vertical mixing play on the dynamics of lake ecosystem.

Model Description

GLM incorporates a flexible Lagrangian layer structure similar to the approach of several 1-D lake model designs (Imberger and Patterson 1981; Hamilton and Schladow 1997; Gal et al. 2003). The Lagrangian design allows for layers to change thickness by contracting and expanding in response to inflows, outflows, mixing and surface mass fluxes. When sufficient energy becomes available to overcome density gradients, two layers will merge thus accounting for the process of mixing. Layer thicknesses are adjusted by the model in order to sufficiently resolve the vertical density gradient. Unlike the fixed grid design where mixing algorithms are typically based on vertical velocities, numerical diffusion of the thermocline is limited, making the GLM approach particularly suited to long-term investigations.

Although GLM is a new model code, many of the heating and mixing algorithms have been based on equations presented by Hamilton and Schladow (1997). GLM has been written with a modernised code structure and features a number of customisations to take advantage of recent advances in the field of numerical hydrodynamics.

Layer structure

The model is composed of a series of layers numbered from the lake bottom to the surface. The number of layers is adjusted to maintain the assumption that each layer must have homogenous properties across the layer. Initially, the layers are assumed to be of equal thickness, and the initial number of layers, $NLEV(0)$, depends on the user-defined minimum and maximum layer thickness limits set, and the lake depth (both defined in `glm.nml`, see model setup section). As the model progresses through time, density changes due to surface heating, vertical mixing, and inflows and outflows lead to dynamic changes in the layer structure. The number of layers will change over time, so that $NLEV = NLEV(t)$. The layer thicknesses will also change each time step as layers expand or contract, maintaining the maximum thickness required to resolve the vertical density gradient.

Energy Budget

A balance of shortwave radiation fluxes, net long wave radiation fluxes, sensible heat and latent heat of evaporative fluxes determine the net cooling and heating for GLM. The model accounts for the surface fluxes of sensible heat and latent heat using commonly adopted bulk aerodynamic formulae.

For sensible heat:

$$\phi_H = -\rho_a c_p C_H U_x (T_a - T_s) \quad (1)$$

where c_p is, C_H is the bulk aerodynamic coefficient for sensible heat transfer ($=1.3 \times 10^{-3}$), T_a the air temperature ($^{\circ}\text{C}$) and T_s the temperature of the surface layer ($^{\circ}\text{C}$).

For latent heat:

$$\phi_E = -\rho_a C_E U_x (e_a[T_a] - e_s[T_s]) \quad (2)$$

where C_E is the bulk aerodynamic coefficient for latent heat transfer, e_a the air vapour pressure and e_s the saturation vapour pressure at the surface layer temperature (hPa). The vapour pressure can be calculated by the following formulae:

$$e_s[T_s] = \exp \left[2.303 \left(7.5 \frac{T_s}{T_s + 273.15} \right) + 0.7858 \right] \quad \text{Option 1} \quad (3)$$

$$e_s[T_s] = 10^{\left(9.28603523 \frac{2322.37885 T_s}{T_s + 273.15} \right)} \quad \text{Option 2}$$

$$e_a[T_a] = \frac{RH}{100} e_s[T_a]$$

Energy fluxes to account for shortwave and longwave radiation are also included in the model. Shortwave radiation is able to penetrate according to the Beer-Lambert Law, and longwave radiation can either be specified as net flux, or incoming flux. The incoming flux may be specified directly or calculated by the model based on the cloud cover fraction and air temperature.

Short wave radiation is calculated as:

$$\phi_{SW}(z) = (1 - \alpha_{SW}) \hat{\phi}_{SW} \exp[-K_d z] \quad (4)$$

$$\alpha_{SW} = \begin{cases} 0.08 + 0.02 \sin \left[\frac{2\pi}{365} d - \frac{\pi}{2} \right] & : \text{northern hemisphere} \\ 0.08 & : \text{equator} \\ 0.08 - 0.02 \sin \left[\frac{2\pi}{365} d - \frac{\pi}{2} \right] & : \text{southern hemisphere} \end{cases} \quad (5)$$

Where $\phi_{SW}(z)$ is the short-wave radiation at depth, z (m), α_{SW} is used to account for the effect of albedo on the penetration of ϕ_{SW} and d is the day of the year

Long wave radiation is calculated as:

$$\phi_{LW_{in}} = \sigma [T_a + 273.15]^4 \times (1 + c_1 C) \times (1 - c_2 \exp[-c_3 T_a^2]) \quad (6)$$

$$\phi_{LW_{out}} = \varepsilon_w \sigma [T_s + 273.15]^4$$

$$\phi_{LW_{net}} = \phi_{LW_{in}} - \phi_{LW_{out}}$$

where σ is the Stefan-Boltzman constant, C the cloud cover fraction (0-1), ε_w the emissivity of the water surface and constants, $c_1 = 0.275$; $c_2 = 0.261$; $c_3 = 0.000777 \times 10^{-4}$.

Surface Mass Fluxes

The model accounts for surface mass fluxes of evaporation, rainfall and snowfall (m day^{-1}):

$$\frac{dh_s}{dt} = \lambda \phi_E + R + S$$

where h_s is the height of the surface layer (m), t time step (s), λ latent heat of evaporation. Note that this equation does not include changes to h_s as a result of mixing dynamics or ice formation/melt as described in the following sections.

Snow/Ice Model

The algorithms for GLM ice and snow dynamics are based on previous ice modelling studies (Patterson and Hamblin, 1988; Gu and Stefan, 1993; Rogers *et al.*, 1995; Vavrus *et al.*, 1996). To solve the heat transfer equation, the ice model uses a quasi---steady assumption that the time scale for heat conduction through the ice is short relative to the time scale of meteorological forcing (Patterson and Hamblin, 1988; Rogers *et al.*, 1995).

The steady---state conduction equations, which allocate shortwave radiation into two components, a visible (A1=70%) and an infra---red (A2=30%) spectral band, are used with a three---component ice model that includes blue ice, snow ice and snow (see Eq. 1 and Fig. 5 of Rogers *et al.*, 1995). Snow ice is generated in response to flooding, when the mass of snow that can be supported by the ice cover is exceeded (see Eq. 13 of Rogers *et al.*, 1995). By assigning appropriate boundary conditions to the interfaces and solving the quasi---steady state of heat transfer numerically, one can determine the upward conductive heat flux between the ice or snow cover and the atmosphere, ϕ_0 . The estimation of ϕ_0 involves the application of an empirical equation (Ashton, 1986) to estimate snow conductivity (Ks) from its density, where the density of snow is determined as outlined in Figure 1.

At the ice (or snow) surface, a heat flux balance is employed to provide the condition for surface melting,

$$\begin{aligned}\phi_0(T_0) + \phi_{net}(T_0) &= 0 & T_0 < T_m \\ &= -\rho L \frac{dh_i}{dt} & T_0 = T_m\end{aligned}$$

where L is the latent heat of fusion (see physical constants, Table 2), h_i is the height of the upper snow or ice layer, t is time, ρ_i is the density of the snow or ice, determined from the surface medium properties, T_0 is the temperature at the solid surface, T_m is the melt-water temperature (0°C) and $\phi_{net}(T_0)$ is the net incoming heat flux, at the solid surface.

$$\phi_{net}(T_0) = \phi_{LWin} - \phi_{LWout}(T_0) + \phi_H(T_0) + \phi_E(T_0) + \phi_R(T_0)$$

where ϕ_{LWin} and ϕ_{LWout} are incoming and outgoing longwave radiation, ϕ_H and ϕ_E are sensible and evaporative heat fluxes between the solid boundary and the atmosphere, and ϕ_R is the heat flux due to rainfall. These heat fluxes are calculated as above with modification for determination of vapor pressure over ice or snow (Gill, 1982) and the addition of the rainfall heat flux (Rogers *et al.*, 1995). T_0 is determined using a bilinear iteration until surface heat fluxes are balanced (i.e. $\phi_0(T_0) = -\phi_{net}(T_0)$) and T_0 is stable ($\pm 0.001^\circ\text{C}$). In the presence of ice (or snow) cover, surface temperature $T_0 > T_m$ indicates that energy is available for melting. The amount of energy for melting is calculated by setting $T_0 = T_m$ to determine the reduced thickness of snow or ice (as shown in Eq. 1).

Accretion or ablation of ice is determined through the heat flux at the ice-water interface, q_f . Solving for heat conduction through ice yields:

$$q_f = q_0 - A_1 I_0 \{1 - \exp(-\lambda_{s1} h_s - \lambda_{e1} h_e - \lambda_{i1} h_i)\} - A_2 I_0 \{1 - \exp(-\lambda_{s2} h_s - \lambda_{e2} h_e - \lambda_{i2} h_i)\} - Q_{si} h_s,$$

where I_0 is the shortwave radiation penetrating the surface, l and h are the light attenuation coefficient and thickness of the ice and snow components designated with subscripts s , i and e for snow, blue ice and snow ice respectively, and Q_{si} is a volumetric heat flux for formation of snow ice, which is given in Eq. 14 of Rogers *et al.* (1995). In this study we fix the ice and snow light attenuation coefficients to the same values as those given by Rogers *et al.* (1995), noting the close agreement to measured values for our study lake. Reflection of shortwave radiation from the ice or snow surface is a function of surface temperature and ice and snow thickness (see Table 2, Vavrus *et al.*, 1996). Values of albedo are derived from these functions vary from 0.08 to 0.6 for ice and from 0.08 to 0.7 for snow.

The imbalance between q_f and the heat flux from the water to the ice, q_w , gives the rate of change of ice thickness at the interface with water:

$$\frac{dh_i}{dt} = \frac{q_f - q_w}{\rho_i L},$$

where ρ_i is the density of blue ice and q_w is given by a finite difference approximation of the conductive heat flux from water to ice:

$$q_w = -K_w \frac{\Delta T}{\Delta z},$$

where K_w is molecular conductivity and ΔT is the temperature difference between the surface water and the bottom of the ice, which occurs across an assigned depth Δz . A value for Δz of 0.5 m is usual, based on the reasoning given in Rogers *et al.* (1995) and the typical vertical resolution of a model simulation (0.125 – 1.5 m). Note that a wide variation in techniques and values is used to determine the basal heat flux immediately beneath the ice pack (e.g., Harvey, 1990).

Figure 1 shows the overall decision tree to update ice cover, snow cover and water depth. The ice cover equations are applied when water temperature first drops below 0 °C. The ice thickness is set to its minimum value of 0.05 m, which is suggested by Patterson and Hamblin (1988) and Vavrus *et al.* (1996). The need for a minimum ice thickness relates primarily to horizontal variability of ice cover during the formation and closure periods. The ice cover equations are discontinued and open water conditions are restored in the model when the thermodynamic balance first produces ice thickness < 0.05 m. The effects of snowfall, rainfall, and compaction of snow are described through appropriate choice of one of several options, depending on the air temperature and whether ice or snow is the upper boundary (Figure 1).

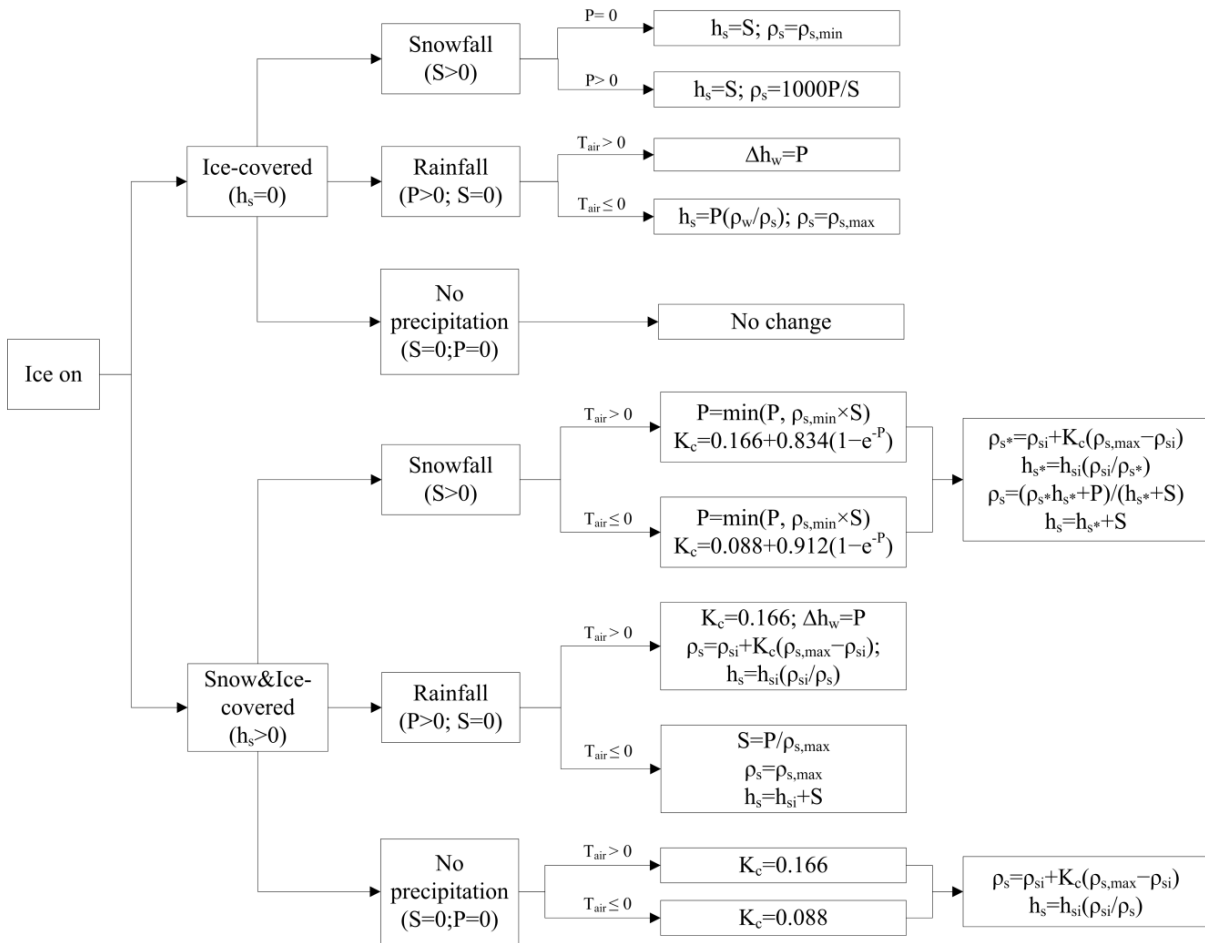


Figure 1: Decision tree to update ice cover, snow cover and water depth according to snow compaction, rainfall (P) and snowfall (S) on each day, and depth of snow cover (h_{si}) and snow density (ρ_{si}) for the previous day. Refer to Table 1 for definitions of other variables.

Density of fresh snowfall is determined as the ratio of measured snowfall height to water-equivalent height, with any values exceeding the assigned maximum snow density ($r_{max} = 300 \text{ kg m}^{-3}$) truncated to the upper limit. The snow compaction model is based on the exponential decay formula of McKay (1968), with selection of snow compaction parameters based on air temperature (Rogers *et al.*, 1995) as well as on rainfall or snowfall. The approach of snow compaction used by Rogers *et al.* (1995) is to set the residual snow density to its maximum value when there is fresh snowfall. This method is found to produce increases in snow density that are too rapid when there is only light snowfall. As a result a gradual approach to increasing snow compaction is adopted.

Vertical mixing

The GLM works on the premise that the balance between the available energy, E_{TKE} , and the required energy to undergo mixing, E_{PE} , provides an equation for the surface mixed layer (SML) deepening rate dh_{mix}/dt . The model calculates the available kinetic energy due to contributions from wind stirring, shear production between layers, convective overturn, and Kelvin-Helmholtz billowing, which combined are summarised according to:

$$E_{TKE} = \underbrace{0.5C_K(w_*^2) \Delta t}_{\text{convective overturn}} + \underbrace{0.5C_W(\psi^3 u_*^3) \Delta t}_{\text{wind stirring}} + \underbrace{0.5 C_S \left[u_b^2 + \frac{u_b^2}{6} \frac{d\xi}{dh} + \frac{u_b \xi}{3} \frac{du_b}{dh} \right]}_{\substack{\text{shear production} \\ \text{K-H production}}} h_{s-1}$$

where u^* and w^* refer to the velocity scales in the horizontal and vertical respectively. The energy required to lift up water at the bottom of the mixed layer, denoted here as layer $i-1$, with thickness h_{i-1} and accelerate it to the SML velocity is required for mixing to occur. This also accounts for energy consumption associated with K-H production and expressed as, E_{PE} :

$$E_{PE} = \left[\underbrace{0.5C_T(w_*^3 + \psi^3 u_*^3)^{2/3}}_{\text{acceleration}} + \underbrace{\frac{\Delta \rho g h_{mix}}{\rho_o}}_{\text{lifting}} + \underbrace{\frac{g \xi^2}{24 \rho_o} \frac{d(\Delta \rho)}{dh} + \frac{g \xi \Delta \rho}{12 \rho_o} \frac{d\xi}{dh}}_{\text{K-H consumption}} \right] h_{s-1}$$

for these, the length scale of the K-H billows is summarised as:

$$\xi = KH \frac{\rho_o u_b^2}{g \Delta \rho}$$

and the velocity of the lower layer is approximated from:

$$u_b = \frac{u_*^2 t}{h_{mix}} + u_o$$

The model first calculates these energy arguments and then loops through layers from the top to the bottom until there is insufficient energy available to lift up the next i^{th} layer.

Mixing below the SML is modelled using a characteristic diffusivity, $K = K_\epsilon + K_m$, based on

$$K_\epsilon = \frac{\alpha_{TKE} \epsilon_{TKE}}{N^2 + 0.6 k_{TKE}^2 u_*^2}$$

and K_m is the fixed molecular diffusivity of scalars. $\alpha = 0.5$ and k is the wavenumber

$$\epsilon_{TKE} = \begin{cases} \epsilon & z_i < (H_t - h_{mix}) \\ \epsilon \exp \left[-\frac{H - h_{mix} - z}{h_{sig}} \right] & z_i < (H_t - h_{mix}) \end{cases}$$

where h_{sig} is the first moment distance of the N^2 distribution below h_{s-1} where N^2 is the buoyancy frequency:

$$N^2 = \frac{g\Delta\rho}{\rho\Delta z}$$

Inflows and outflows

Any number of inflows to the domain can be specified and these are applied at the end of the sub-daily loop, i.e. once a day. Depending on the density of the river water, the inflow will form a positive or negatively buoyant intrusion. As the inflow crosses layers it will entrain water until it reaches a level of neutral buoyancy. At its point of neutral buoyancy it is then assumed to insert as a new layer of thickness depending on the inflow volume at that time (including the effects of entrainment); it may then amalgamate with adjacent layers depending on numerical criteria within the model.

The model operates by estimating the increase in inflow thickness due to entrainment by:

$$h_i = 1.2Edx + h_{i-1}$$

where h_i is the inflow thickness, E is the entrainment rate and dx is the distance travelled by the inflowing water, calculated from the flow rate and inflow thickness. For the initial calculation:

$$h_0 = \left(2Q_i^2 \frac{Ri}{g'} \tan^2 \beta\right)^{0.2}$$

where Q is the flow rate provided as a boundary condition, Ri is the Richardson number, g' is reduced gravity and β is the slope of the inflow at the point where it meets the water body. The flow is estimated to increase according to:

$$Q_i = Q_{i-1} \left[\left(\frac{h_i}{h_{i-1}} \right)^{5/3} - 1 \right]$$

and E is calculated from either:

$$E = \frac{3}{4} \left[\frac{5 \tan \Phi}{F^2} - \frac{5C_D}{\sin \beta} \right] \frac{F^2}{(3F^2 + 2)}$$

or:

$$E = 1.6 \frac{C_D^{1.5}}{Ri}$$

where C_D is the user specified drag coefficient for the inflow and Ri of the inflow is estimated from:

$$Ri = \frac{C_D \left(1 + 0.21C_D \sin \left[\frac{\beta\pi}{180} \right] \right)}{\sin \left[\frac{\beta\pi}{180} \right] \sin \left[\frac{\Phi\pi}{180} \right] / \cos \left[\frac{\Phi\pi}{180} \right]}$$

Outflows can be specified at any depth over the water column and they are accounted for by removing water from the layer at the depth defined at the outlet point and computation of the Grashof number:

$$Gr = \frac{N^2 A_i^2}{\nu^2}$$

Model Input Data Requirements

The model requires the user to supply a hypsographic curve $A = A(h)$ to describe the storage, elevation, area & volume relationship, meteorological time-series data for surface forcing, and daily time-series of volumetric inflow and outflow rates. Further details of the model setup and file formats are outlined in the GLM Setup section. A summary of relevant parameters within the model and their default values are summarised below in Table 1.

Table 1. Summary of GLM physical parameters with recommended values and references.

Symbol	glm.nml ID	Description	Units	Default	Reference	Comments
Model Structure						
h_{min}	min_layer_thick	Minimum layer thickness	m	0.5	-	Standardised for multi-lake comparison
h_{max}	max_layer_thick	Maximum layer thickness	m	2	-	Standardised for multi-lake comparison
Lake Properties						
K_w	Kw	Extinction coefficient for shortwave radiation	m^{-1}	none	Lake specific	Should be measured, e.g. mean of simulation period
Surface Exchange						
C_H	ch	Bulk aerodynamic coefficient for sensible heat transfer	-	0.0014	Fischer et al. 1979	From Hicks' (1972) collation of ocean and lake data
C_E	ce	Bulk aerodynamic coefficient for latent heat transfer	-	0.0013	Fischer et al. 1979	From Hicks' (1972) collation of ocean and lake data
C_M	coef_wind_drag	Bulk aerodynamic coefficient for transfer of momentum	-	0.0013	Fischer et al. 1979	From Hicks' (1972) collation of ocean and lake data
Mixing Parameters						
C_K	coef_mix_conv	Mixing efficiency - convective overturn	-	0.2	Yeates & Imberger 2003	Selected by Yeates.. from a range given in Spigel et al. (1986)
C_W	coef_wind_stir	Mixing efficiency - wind stirring	-	0.23	Spigel et al. 1986	From Wu 1973
C_S	coef_mix_shear	Mixing efficiency - shear production	-	0.3	Sherman et al. 1978	Best fit of experiments reviewed
C_T	coef_mix_turb	Mixing efficiency - unsteady turbulence (acceleration)	-	0.51	DLM manual	..need to verify this
KH	coef_mix_KH	Mixing efficiency - Kelvin-Helmholtz turbulent billows	-	0.3	Sherman et al. 1978	"a good rule of thumb..."
α_{TKE}	coef_mix_hyp	Mixing efficiency of hypolimnetic turbulence	-	0.5	GLM 1.2.0 code	
Other						
C_D	strmbd_drag	streambed_drag	-	0.016	-	Source unknown
u_{out}	-	Maximum withdrawal velocity	$m\ s^{-1}$		GLM 1.2.0 code	Not adjustable in GLM.nml
Physical constants						
λ	-	Latent heat of evaporation	$J\ kg^{-1}$	2.453E+06	GLM 1.2.0 code	Not adjustable in GLM.nml
ϵ	-	Emissivity of the water surface	-	0.97 0.95	GLM 1.2.0 code	no ice ice or snow
σ	-	Stefan-Boltzmann constant	$W\ m^{-2}\ K^{-4}$	5.67E-08	GLM 1.2.0 code	Not adjustable in GLM.nml

Table 2. Summary of ice model parameter descriptions, units and typical values.

Symbol	Description	Units	Default value	Comment
I_{e1}	Waveband 1, snow ice light extinction	m^{-1}	48.0	
I_{e2}	Waveband 2, snow ice light extinction	m^{-1}	20.0	
I_{i1}	Waveband 1, blue ice light extinction	m^{-1}	1.5	
I_{i2}	Waveband 2, blue ice light extinction	m^{-1}	20.0	
I_{s1}	Waveband 1, snow light extinction	m^{-1}	6	
I_{s2}	Waveband 2, snow light extinction	m^{-1}	20	
D_z	Distance of heat transfer, ice water	m	0.039	
r_e	Density, snow ice	kg m^{-3}	890	
r_i	Density, blue ice	kg m^{-3}	917	
r_s	Density, snow	kg m^{-3}	Variable	
c_{pi}	Heat capacity, ice	$\text{kJ kg}^{-1} \text{ } ^\circ\text{C}^{-1}$	2.1	
c_{pw}	Heat capacity, ice	$\text{kJ kg}^{-1} \text{ } ^\circ\text{C}^{-1}$	4.2	
K_c	Compaction coefficient	-	Variable	
K_e	Thermal conductivity, snow ice	$\text{W m}^{-1} \text{ } ^\circ\text{C}^{-1}$	2.0	
K_e	Thermal conductivity, blue ice	$\text{W m}^{-1} \text{ } ^\circ\text{C}^{-1}$	2.3	
K_e	Thermal conductivity, snow	$\text{W m}^{-1} \text{ } ^\circ\text{C}^{-1}$	Variable	
K_e	Thermal conductivity, sediment	$\text{W m}^{-1} \text{ } ^\circ\text{C}^{-1}$	1.2	
K_e	Thermal conductivity, water	$\text{W m}^{-1} \text{ } ^\circ\text{C}^{-1}$	0.57	
L	Latent heat of fusion	kJ kg^{-1}	0334	

GLM-FABM-AED Setup

Overview

Here a description of the structure of a GLM setup is described. The GLM requires a configuration files and several time-series input files.

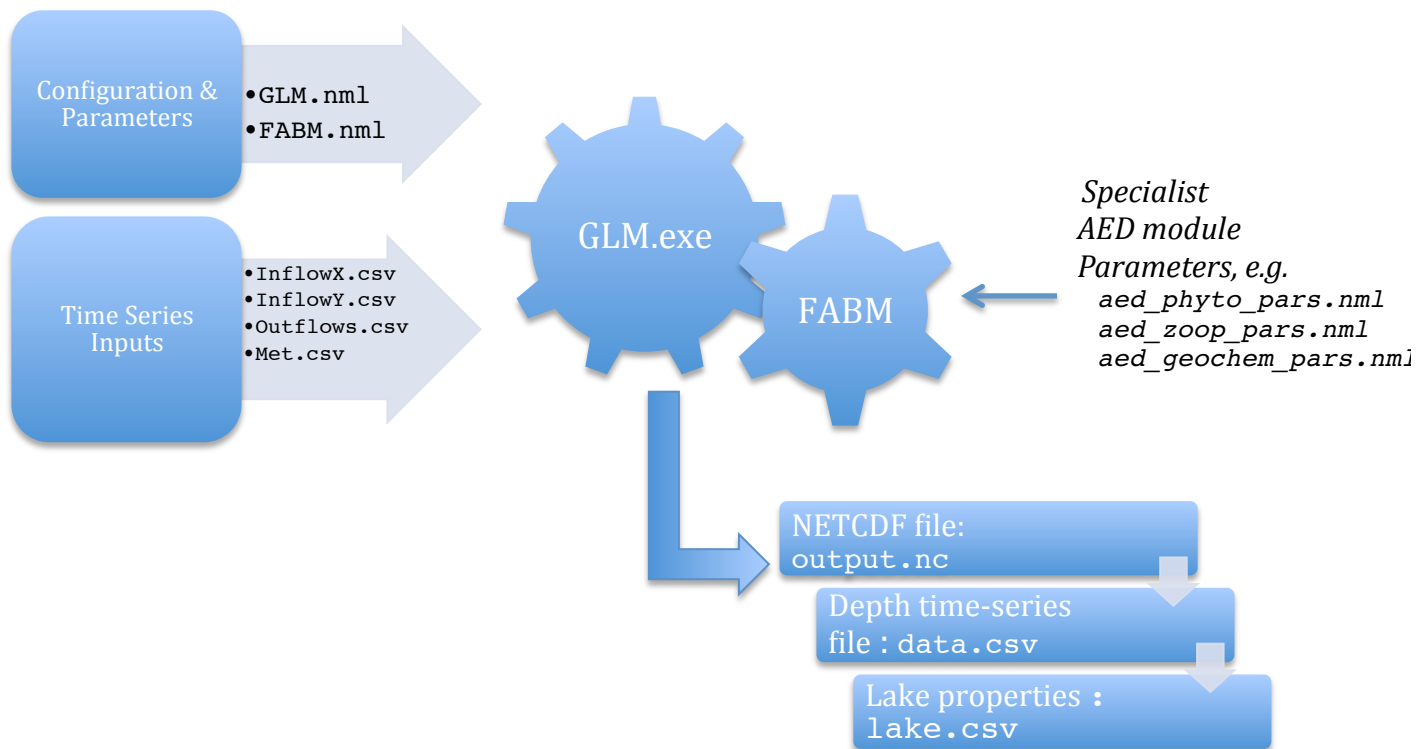


Figure 3: Flow diagram showing the files required for operation of the model.

Input files

Physical model configuration: glm.nml

The file glm.nml is the main configuration file for the physical model, and some details related to the FABM coupling. The nml file includes detailed description of the different namelist options for each block; if these value are not present default values will be assumed. It is a namelist file with blocks for:

- `&glm_setup:` General simulation info
- `&fabm_setup:` Details about the FABM coupling
- `&time:` Time controls
- `&morphometry:` Lake morphometric information
- `&output:` Output file details
- `&init_profiles:` Initial profiles
- `&meteorology:` Information about surface forcing and meteorology data
- `&inflows:` Information about inflows
- `&outflows:` Information about outflows

Meteorology: met . csv

The meteorological conditions are provided as a daily time-series of data with a fixed number of columns, as outlined in Table C. In future version sub-daily inputs will be supported. It contains seven compulsory columns, and several optional columns after these depending on the user-defined configuration switches for `snow_sw` and `rain_sw` in the `glm.nml` file.

Table 3: Flow diagram showing the files required for operation of the model.

Met.csv column	Units	Description
(1) TIME	YYYY-MM-DD	Date
(2) SHORTWAVE RADIATION	W/m ²	Daily average shortwave radiation. Note that the daily value is internally distributed to a sub-daily time step by assuming an idealized diurnal cycle.
(3) LONGWAVE RADIATION	W/m ² if <code>lw_type</code> = LW_IN or LW_NET or 0 – 1 if <code>lw_type</code> = LW_CC	Longwave radiation input is either direct incident intensity, net longwave flux, or estimated from cloud cover fraction.
(4) AIR TEMPERATURE	°C	Daily average air temperature 10m above the water surface
(5) RELATIVE HUMIDITY	%	Daily average relative humidity (0-100%) 10m above the water surface.
(6) WIND SPEED	m/s	Daily average wind speed 10m above the water surface
(7) RAINFALL	m/day	Daily rainfall depth
(8) SNOWFALL (optional)	m/day	Daily snowfall depth (optional – include if <code>snow_sw</code> is T)
(9-14) RAINFALL WQ DEPOSITION CONCENTRATIONS (optional)	mg/L	... (optional – include if <code>rain_sw</code> is T)

Inflows: `inflows.csv`

Any number of inflows can be simulated by the model with the configuration and filenames set in the `glm.nml` file. For each inflow there is an associated inflow file of the format outlined in Table X. At this stage the file only expects daily data as the inflow calculation is done once a day. It contains four compulsory columns for time, flow, temperature and salinity, and optional columns for FABM constituents.

Table 4: Flow diagram showing the files required for operation of the model.

Inflow.csv column	Units	Description
(1) <i>TIME</i>	YYYY-MM-DD	Date
(2) <i>INFLOW</i>	ML/day	Daily flow rate. Convert from m ³ /s by multiplying by 86.4.
(3) <i>STREAMFLOW TEMPERATURE</i>	°C	Average daily streamflow temperature
(4) <i>STREAMFLOW SALINITY</i>	mg/L	Average daily streamflow salinity
(5 ... $n_{wq}+4$) <i>STREAMFLOW FABM PARAMETER CONCENTRATIONS</i>	mmol/m ³	Average daily streamflow FABM constituent concentrations.

Outflows: `outflows.csv`

Any number of outflow fluxes can be configured and these are set as consecutive columns in the file `outflows.csv` (Table X). Only daily flow rates are required and FABM variables are not required.

Table 5: Flow diagram showing the files required for operation of the model.

Outflow.csv column	Units	Description
(1) <i>TIME</i>	YYYY-MM-DD	Date
(2 ... $n_{out}+1$) <i>OUTFLOW</i>	ML/day	Daily outflow rates of each outflow

Running the model

The model may be run by navigating to the directory where the `glm.nml` and `fabm.nml` files are and executing the model executable `glm.exe`. This can be located in different directory and added to the system path if desired.

Windows users may wish to add the command into a `glm.bat`:

```
..\bin\glm.exe >glm.log
```

which will create a file that can simply be double-clicked from windows explorer. The model will output to the netcdf and/or csv files which can then be plotted.

Outputs and post-processing

The model includes several types of outputs, including the NETCDF file, an optional csv time-series file at a certain point, and an optional live contour plot as the model runs to enable the modeller to monitor simulation progress.

Live output plotting: `plots.nml`

If the model is run with the optional command line argument “`--xdisp`” then the model will display live plots of output parameters. The number of plots, parameters to plot and the colour bar limits are set in the file `plots.nml`.

```
&plots
  nplots = 4
  plot_width = 400
  plot_height = 200
  title = 'Temperature','Salinity','DO','Green'
  vars = 'temp','salt','aed_oxygen_oxy','aed_phytoplankton_green'
  min_z = 0.0, 0.0, 0.0, 0.0
  max_z = 27.0, 0.91, 800.0, 20.0
/
```

Plotting in EXCEL

For simple time-series plots, the user can configure outputs from the model directly to a csv file for a certain depth (defined relative to the bottom, or from the surface), and this information is defined in the `glm.nml` `&output` section. The columns to plot must also be listed here and are user-definable.

Plotting in MATLAB

For more advanced or customised plots, then the user may load the `output.nc` NETCDF file into MATLAB. Recent versions of MATLAB (MATLAB 2011a or after) natively support NETCDF and can load the file directly. An example MATLAB script for plotting is shown below: and produces figures as in Figure X.

```
foldername = '../MyGLMSim/';
outname = '../ MyGLMSim /figures /';
mkdir([outname]);

data = nldncGLM([foldername,'/output.nc'])

varNames = names_netcdf([foldername,'output.nc']);
varsToPlot = varNames([20:64]);

for ii = 1:length(varsToPlot)
```

```
newFig = plotGLM(varsToPlot{ii},data);  
  
figName = [outname,'/', varsToPlot {ii},'.png'];  
print(gcf,'-dpng', figName,'-opengl');  
close all  
end
```

Further a simple GLM-FABM plotting GUI is also available.

Plotting with PyNCview

Not yet supported.

Parameter Optimisation

TBC

Examples & Support

Downloads & Online Forum

To download the model, visit: glm.gleon.org

Support and FAQ's are available at the Aquatic Ecosystem Modelling Network (AEMON) website:

<http://sites.google.com/site/aquaticmodelling/>

Further Support & Development Requests

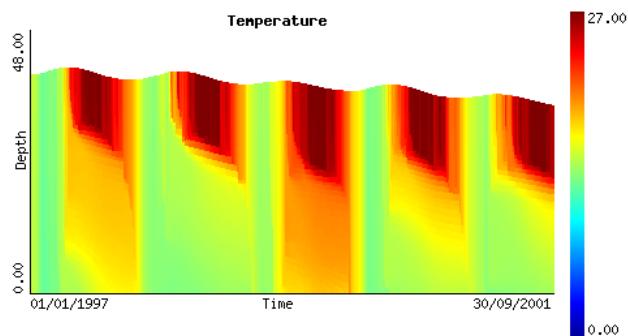
Please contact Dr Louise Bruce, or A/Prof Matthew Hipsey
School of Earth and Environment
The University of Western Australia

louise.bruce@uwa.edu.au

matt.hipsey@uwa.edu.au

Examples

Lake Kinneret



Lake Constance

References

- Ambrose, R.B. Jr., Wool, T.A., Conolly, J.P., and Scahnz, R.W.. 1988. A Hydrodynamic and Water Quality Model: Model Theory, Users Manual, and Programmers manual: WASP4 Environmental Research Laboratory, US EPA, EPA 600/3-87/039, Athens, GA.
- Arhonditsis, G.B., Adams-Vanharn, B.A., Nielsen, L., Stow, C.A., and Reckhow, K.H., 2006. Evaluation of the current state of mechanistic aquatic biogeochemical modeling: citation analysis and future perspectives. *Environ. Sci. Technol.*, **40**, 6547-6554.
- Arhonditsis, G.B., M.T. Brett. 2004. Evaluation of the current state of mechanistic aquatic biogeochemical modeling. *Marine Ecology Progress Series*, **271**: p. 13–26.
- Bruce, L.C., Hipsey, M.R. and Cook, P.M., Quantification of sediment and water processing of nitrogen in a periodically anoxic urban estuary using a 3D hydrodynamic-biogeochemical model. Submitted to *Journal of Soils and Sediments*.
- Bruce LC, Hamilton DP, Imberger J, Gal G, Gophen M, Zohary T, Hambright KD, 2006. A numerical simulation of the role of zooplankton in C, N and P cycling in Lake Kinneret, Israel. *Ecol. Model.* **193**:412-436.
- Broekhuizen, N., Rickard, G. J., Bruggeman, J. & Meister, A. 2008. An improved and generalized second order, unconditionally positive, mass conserving integration scheme for biochemical systems. *Applied Numerical Mathematics* 58:319–40.
- Bruggeman, J. 2011. D2.14 Users guide and report for models in the MEECE library – Framework for Aquatic Biogeochemical Models (FABM). Report for the EC FP7 MEECE project 212085. 57pp.
- Burchard H et al. 2005. Application of modified Patankar schemes to stiff biogeochemical models, *Ocean Dyn*, **55**: 326-37
- Burchard, H., Bolding, K., Kuhn, W., Meister, A., Neumann, T. & Umlauf, L. 2006. Description of a flexible and extendable physical-biogeochemical model system for the water column. *Journal of Marine Systems* 61: 180-211.
- Chao, X., Jia, Y., Shields, F.D., Wang, S.S.Y., and Cooper, C.M., 2010. Three-dimensional numerical simulation of water quality and sediment-associated processes with application to a Mississippi Delta lake. *Journal of Environmental Management* **91**: 1456 – 1466.
- Coles, J.F. and R.C. Jones. 2000. Effect of temperature on photosynthesis-light response and growth of four phytoplankton species isolated from a tidal freshwater river. *J. Phycology*, **36**: 7-16.
- Droop, M.R. 1974. The nutrient status of algal cells in continuous culture. *J. Mar. Biol. Assoc. UK*, **54**: 825–855.
- Fasham, M.J.R., Ducklow, H.W. & Mckelvie, S.M., 1990. A nitrogen-based model of plankton dynamics in the oceanic mixed layer. *J Mar Res* 48: 591-639
- Gal, G., Hipsey, M.R., Paparov, A., Makler, V. and Zohary, T., 2009. Implementation of ecological modeling as an effective management and investigation tool: Lake Kinneret as a case study. *Ecol. Model.*, **220**: 1697-1718.
- Kilminster et al., 2011. Unpublished data.
- Romero, J.R., Antenucci, J.P., & Imberger, J. 2004. One- and Three- Dimensional biogeochemical Simulations of Two Differing Reservoirs. *Ecol. Model.*.
- Riley, J.P. & Skirrow, G.. 1974. *Chemical Oceanography* Academic Press, London.
- Robarts, R.D. and T. Zohary. 1987. Temperature effects on photosynthetic capacity, respiration and growth rates of bloom forming cyanobacteria. *N.Z. J Mar. Freshwater Res.* **21**: 391-399.
- Schladow, S.G. & Hamilton, D.P. 1997 Water quality in lakes and reservoirs. Part II Model calibration, sensitivity analysis and application. *Ecol. Model.* **96**: 111–123.
- Rhee, G.Y. & Gotham, E.J. 1981 The effect of environmental factors on phytoplankton growth: temperature and the interactions of temperature with nutrient limitation. *Limnol. Oceanogr.* **26**, pp. 635–648.
- Jellison, R. & Melack, J.M. 1993. Meromixis and vertical diffusivities in hypersaline Mono Lake, California. *Limnol. Oceanogr.* **38**: 1008–1019.
- Kromkamp, J. & Walsby, A.E. 1990. A computer model of buoyancy and vertical migration in cyanobacteria. *J. Plankton Res.* **12**: 191–183.
- Griffin, S.L., Herzfeld, M., Hamilton, D.P., 2001. Modelling the impact of zooplankton grazing on phytoplankton biomass during a dinoflagellate bloom in the Swan River Estuary, Western Australia. *Ecological Engineering*, **16**: 373-394.
- Hamilton, D.P. & Schladow, S.G. 1997. Water quality in lakes and reservoirs. Part I Model description. *Ecol. Model.* **96**: 91–110.

- Hipsey, M.R., Salmon, S.U., Aldrige, K.T. and Brookes, J.D., 2010. Impact of hydro-climatological change and flow regulation on physical and biogeochemical dynamics of the Lower River Murray, Australia. *8th International Symposium on Ecohydraulics (ISE2010)*, September, 2010, Korea.
- Kruger, G.H.J. and J.N. Eloff. 1977. The influence of light intensity on the growth of different *Microcystis* isolates. *J. Limnol. Soc. Sth Africa*. **3**: 21-25.
- Imberger, J. and J.C. Patterson. 1981. A dynamic reservoir simulation model-DYRESM:5. In *"Transport Models for Inland and Coastal Waters."* H.B. Fisher(ed). Academic Press, New York. : 310-361.
- Mooij, W.M., Trolle, D., Jeppesen, E., Arhonditsis, G., Belolipetsky, P.V., Chitamwebwa, D.B.R., Degermendzhy, A.G., DeAngelis, D.L., De Senerpont Domis, L.N., Downing, A.S., Elliott, A.E., Fragoso Jr, C.R., Gaedke, U., Genova, S.N., Gulati, R.D., Håkanson, L., Hamilton, D.P., Hipsey, M.R., Hoen, J., Hülsmann, S., Los, F.J., Makler-Pick, V., Petzoldt, T., Prokopkin, I.G., Rinke, K., Schep, S.A., Tominaga, K., Van Dam, A.A., Van Nes, E.H., Wells, S.A., Janse, J.H., 2010. Challenges and opportunities for integrating lake ecosystem modelling approaches, *Aquatic Ecology*, **44**: 633–667.
- Petrone K.C. Richards, J.S. and Grierson, P.F., 2009. Bioavailability and composition of dissolved organic carbon and nitrogen in a near coastal catchment of south-western Australia. *Biogeochemistry*, **92**: 27-40.
- Smith, C.S., Haese, R.R. and Evans, S. 2010. Oxygen demand and nutrient release from sediments in the upper Swan River estuary. *Geoscience Australia Record*, 2010/28. Commonwealth Government, Canberra.
- Smith, C.S., Murray, E.J., Hepplewhite, C. and Haese, R.R. (2007. Sediment water interactions in the Swan River estuary: Findings and management implications from benthic nutrient flux surveys, 2000-2006. *Geoscience Australia Record* 2007/13.
- Spillman, C.M., Hamilton, D.P., Hipsey, M.R. and Imberger, J., 2008. A spatially resolved model of seasonal variations in phytoplankton and clam (*Tapes philippinarum*) biomass in Barham Lagoon, Italy, *Estuarine, Coastal and Shelf Science*, **79**: 187-203.
- Spillman, C.M., Imberger, J., Hamilton, D.P., Hipsey, M.R. and Romero, J.R., 2007. Modelling the effects of Po River discharge, internal nutrient cycling and hydrodynamics on biogeochemistry of the Northern Adriatic Sea. *Journal of Marine Systems*, **68**: 127-200.
- Talling, J. F. 1957. The phytoplankton population as a compound photosynthetic system. *New Phytol.* **56**: 133-149
- Trolle, D., Hamilton, D.P., Hipsey, M.R., Bolding, K., Bruggeman, J., Mooij, W. M., Janse, J. H., Nielsen, A., Jeppesen, E., Elliott, J. E., Makler-Pick, V., Petzoldt, T., Rinke, K., Flindt, M. R., Arhonditsis, G.B., Gal, G., Bjerring, R., Tominaga, K., Hoen, J., Downing, A. S., Marques, D. M., Fragoso Jr, C. R., Søndergaard, M. and Hanson, P.C. 2012. A community-based framework for aquatic ecosystem models. *Hydrobiologia*, 683(1): 25-34.
- Wanninkhof, R.. 1992. Relationship between windspeed and gas exchange over the ocean. *J. Geophys. Res. (Oceans)* **97**(C5): 7373–7382.
- Webb, W.L., Newton, M., & Starr, D. 1974. Carbon dioxide exchange of *Alnus rubra*: a mathematical model. *Oecologia* **17**: 281–291.
- Yeates, P.S. and Imberger, J. 2004. Pseudo two-dimensional simulations of internal and boundary fluxes in stratified lakes and reservoirs. *Int. J. Riv. Basin Res.* **1**: 1-23.